Low-frequency plasmons in metallic carbon nanotubes

M. F. Lin and D. S. Chuu
Electrophysics Department, National Chiao Tung University, Hsinchu 30050, Taiwan, Republic of China

K. W.-K. Shung
Physics Department, National Tsing Hua University, Hsinchu 30043, Taiwan, Republic of China
(Received 30 September 1996; revised manuscript received 28 February 1997)

A metallic carbon nanotube could exhibit a low-frequency plasmon, while a semiconducting carbon nanotube or a graphite layer could not. This plasmon is due to the free carriers in the linear subbands intersecting at the Fermi level. The low-frequency plasmon, which corresponds to the vanishing transferred angular momentum, belongs to an acoustic plasmon. For a smaller metallic nanotube, it could exist at larger transferred momenta, and its frequency is higher. Such a plasmon behaves as that in a one-dimensional electron gas (EGS). However, it is very different from the π plasmons in all carbon nanotubes. Intertube Coulomb interactions in a metallic multishell nanotube and a metallic nanotube bundle have been included. They have a strong effect on the low-frequency plasmon. The intertube coupling among coaxial nanotubes markedly modifies the acoustic plasmons in separate metallic nanotubes. When metallic carbon nanotubes are packed in the bundle form, the low-frequency plasmon would change into an optical plasmon, and behave like that in a three-dimensional EGS. Experimental measurements could be used to distinguish metallic and semiconducting carbon nanotubes. [S0163-1829(97)02327-8]

I. INTRODUCTION

Since carbon nanotubes were discovered in 1991 by Iijima,[1] they have stirred much attention. One of the most interesting properties is that the electronic properties are closely related to their geometry. Carbon nanotubes are predicted to be metals or semiconductors,[2–4] which depend on radius (r) and chiral angle (θ). The low-frequency excitations would directly reflect the characteristics of the electronic structure near the Fermi level (E_f). Experimental measurements on them could be used to verify the predicted electronic structure. The objective of this work is to investigate the low-frequency excitations of the carbon nanotubes by means of evaluating the dielectric function (ϵ). For comparison, a single graphite layer is also studied.

A metallic nanotube owns the linear subbands intersecting at the Fermi level. These subbands have a finite density of states at $E_{F,}$ so that the electrons in them would behave as free carriers in normal metals.[2] They have been predicted to make a large contribution to the magnetic,[5–7] transport,[8] and thermal properties.[9] Here, a new low-frequency plasmon is identified in association with them. Semiconducting nanotubes or a graphite layer, which do not have such metallic free carriers, would not exhibit such low-frequency plasmons. Measurements on the low-frequency plasmon by the reflection-electron-energy-loss spectroscopy[10] (REELS) with high resolution $\sim$10 meV would be very useful in distinguishing metallic and semiconducting nanotubes. The dependence of the low-frequency plasmon on the transferred momentum (q), the transferred angular momentum (L), the radius (r), and the intertube Coulomb interactions (see below), will be investigated. The q-dependent behavior of the low-frequency plasmon could help us to understand whether the free carriers in a metallic nanotube behaves as a one-dimensional electron gas[11] (1D EGS) or not. Such a plasmon is very different from the π plasmon in certain respects, e.g., the cause of plasmon. A detailed comparison between them will be discussed.

There are two special features about the carbon nanotubes. One is that nanotubes of different radii and chiral angles may exist coaxially.[1] The intertube Coulomb interactions[12–15] among coaxial nanotubes add unique features that distinguish carbon nanotubes from other quasi-1D systems (e.g., semiconductor quantum wires; QW's).[11] They would play an important role in the low-frequency collective excitations, e.g, the significant modification of the acoustic plasmons in separate nanotubes. Another is that the identical single-shell nanotubes could be uniformly packed in the bundle form. Thess *et al.* recently reported the observation of the metallic nanotube bundle in a 2D triangular lattice.[16] The intertube interaction in a multishell nanotube still exhibits the 1D characteristic [Eq. (3)], but that in a nanotube bundle changes into the 3D characteristic [Eq. (5)]. The low-frequency plasmon in a metallic nanotube bundle is thus expected to differ quite a lot from that in a metallic single-shell or multishell nanotube.

This paper is organized as follows. In Sec. II, the dielectric function is calculated within the self-consistent-field (SCF) approach.[17] The low-frequency excitation properties are discussed in Sec. III. They are studied for a single-shell nanotube, a multishell nanotube, a nanotube bundle, and a graphite sheet. Concluding remarks are given in Sec. V.

II. THE DIELECTRIC FUNCTION

The π band of a carbon nanotube is calculated from the tight-binding model,[4] as done for a graphite sheet.[18] It is simply reviewed in Appendix A. Both energy dispersions and Bloch functions are analytic; therefore, they are convenient in calculating the dielectric function (ϵ). ϵ is evaluated

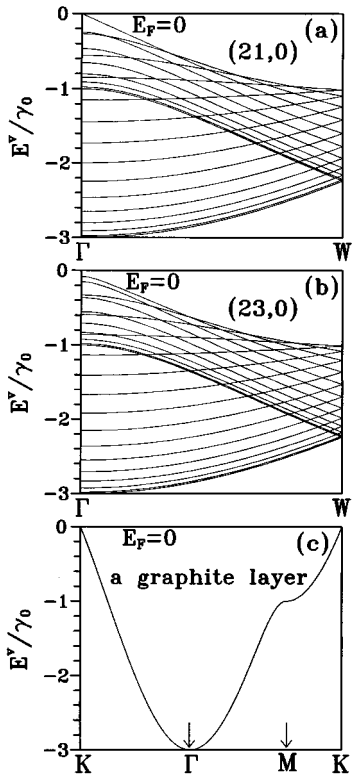

FIG. 1. The π band. (a) The bonding energy bands of the (21,0) nanotube within the first Brillouin zone. The occupied bonding energy bands are symmetric, about $E_F=0$, to the unoccupied antibonding energy bands (not shown). (b) Same plot as (a), but for the (23,0) nanotube. (c) The bonding energy bands of a graphite layer. It is shown along the principal directions in the hexagonal Brillouin zone (Fig. 1 in Ref. 7). Γ, K, and M points are origin, corner, and middle point between two neighboring corners, respectively.

for a single-shell and multishell nanotube, a nanotube bundle, and a graphite sheet. There are obvious differences among them.

A single-shell carbon nanotube[1] could be regarded as a rolled-up graphite sheet in the cylindrical form (details in Ref. 7). A cylindrical (m,n) nanotube is characterized by the radius $r=b\sqrt{3(m^2+mn+n^2)/2\pi}$ ($b=1.42$ Å) and the chiral angle $\theta=\tan^{-1}[-\sqrt{3}n/(2m+n)]$. Within the tight-binding model, a (m,n) nanotube is a metal (semiconductor) when $2m+n=3I$ ($\neq 3I$), where I is an integer. For example, the (21,0) nanotube is a metal [Fig. 1(a)], and the (23,0) nanotube is semiconductor with energy gap 0.48 eV [Fig. 1(b)]. In addition, a single graphite layer is a zero-gap semiconductor [Fig. 1(c)]. A carbon nanotube has many 1D subbands described by discrete angular momenta (J's) and axial wave vectors (k_y's). The occupied bonding energy bands of a carbon nanotube are symmetric, about $E_F=0$, to the unoccupied antibonding energy bands.[4] In general, all 1D subbands have parabolic profiles except that the subbands nearest the Fermi level in a metallic nanotube are linear. The π-band characteristics will be reflected in the electronic excitations. For example, the π-electronic collective excitations with frequency $w_p>2\gamma_0$ (the π plasmons) exist in all carbon nanotubes,[15] which are derived from the excitations of the concave-upward bonding energy bands below $-\gamma_0$ ($=-3.033$ eV).[4] Here, whether the low-frequency plasmon with $w_p<2$ eV exists is mainly determined by the band property near E_F, metal or semiconductor.

As a result of the cylindrical symmetry, the transferred angular momentum and momentum are conserved in the electron-electron interactions.[12–15,19] That is to say, a carbon nanotube could exhibit the L-decoupled excitations, with the q-dependent dispersion relations. This contrasts greatly with the complicated coupling among the interband excitations in an ordinary QW,[11] since the good quantum number L is absent in the latter. At $T=0$, the inter-π-band excitations from the bonding to the antibonding energy bands are the only excitation channel. The dielectric function of a single-shell nanotube, which includes all inter-π-band excitations,[15,17] is expressed by

$$\epsilon(q,L,w)=\epsilon_0-V(q,L)\chi(q,L,w), \tag{1a}$$

$$\chi(q,L,w)=2\sum_J \int_{1\text{st BZ}}\frac{dk_y}{(2\pi)^2} \times|\langle J+L,k_y+q;c|e^{iqy}e^{iL\phi'}|J,k_y;v\rangle|^2 \times\frac{-2w_{vc}(J,k_y;q,L)}{[w_{vc}(J,k_y;q,L)]^2-(w+i\Gamma)^2}, \tag{1b}$$

$w_{vc}(J,k_y;q,L)=E^c(J+L,k_y+q)-E^v(J,k_y)$ is the inter-π-band excitation energy. $\epsilon_0=2.4$ is the background dielectric constant.[20] $V(q,L)=4\pi e^2 I_L(qr)K_L(qr)$ is the Coulomb interaction of a 1D EGS.[12] I_L (K_L) is the first (second) kind of modified Bessel function of the order L. Γ is the energy width due to various de-excitation mechanisms. When Γ is finite, the dielectric function needs to be modified according to Mermin.[21] The low-frequency excitations are mainly due to the $L=0$ mode. The band-structure effects included in the response function $\chi(q,L,w)$ are found to be very important. For example, the π plasmon has $w_p>2\gamma_0$ for any L.[15]

The primary difference in excitation properties between a carbon nanotube and a graphite layer is that L is absent in the latter. However, the dielectric function $[\epsilon(q,\alpha,w)]$ of a graphite layer depends on magnitude (q) and direction (α) of the transferred momentum, owing to the anisotropy of the π band [Fig. 1(c)]. The azimuthal angle α is the angle between the transferred momentum and the x' axis [Fig. 1(a) in Ref. 7]. $\epsilon(q,\alpha,w)$ is given by[17]

$$\epsilon(q,\alpha,w)=\epsilon_0-V(q;2\text{D})\chi(q,\alpha,w), \tag{2a}$$

and

$$\chi(q,\alpha,w)=2\int_{1\text{st BZ}}\frac{dk_{x'}dk_{y'}}{(2\pi)^2}|\langle k_{x'}+q_{x'},k_{y'}+q_{y'};c|e^{iq_{x'}x'}e^{iq_{y'}y'}|k_{x'},k_{y'};v\rangle|^2\frac{2w_{vc}(k_{x'},k_{y'};q,\alpha)}{[w_{vc}(k_{x'},k_{y'},q,\alpha)]^2-(w+i\Gamma)^2}. \tag{2b}$$

$q_{x'}=q\cos\alpha$; $q_{y'}=q\sin\alpha$. $w_{vc}(k_{x'},k_{y'};q,\alpha)=E^c(k_{x'}+q_{x'},k_{y'}+q_{y'})-E^v(k_{x'},k_{y'})$. $V(q;2\mathrm{D})=2\pi e^2/q$ is the Coulomb interaction of a 2D EGS. ϵ in Eq. (2a) could also be used to study the π plasmon in a graphite layer. In addition, the dielectric function in Ref. 22 is only suited to the low-frequency excitations ($w<3$ eV).

The dielectric function [Eq. (1)] of a single-shell nanotube would be modified in the presence of the intertube Coulomb interactions. For a multishell nanotube, q and L are still conserved during the electron-electron interactions.[12–15] The nanotube system is assumed to be perturbed by a probing electron via the time-dependent potential $V^{\mathrm{ex}}(q,L,w)$. Electrons on all shells would screen this external field, which thus causes the induced charges. The induced potential from all induced charges is proportional to the effective potential within the linear-response approximation,[17] in which one of the coefficients is the response function. The effective potential $v_i^{\mathrm{eff}}(q,L,w)$ on the ith shell is given by the linear relations

$$\begin{aligned} v_i^{\mathrm{eff}}(q,L,w)&=v_i^{\mathrm{ex}}(q,L,w)+v_i^{\mathrm{in}}(q,L,w)\\ &\equiv v_i^{\mathrm{ex}}(q,L,w)\\ &\quad+\sum_{j=1}^{N}V(q,L;r_i,r_j)\chi_j(q,L,w)v_j^{\mathrm{eff}}(q,L,w), \end{aligned} \tag{3}$$

where $V(q,L;r_i,r_j)=4\pi e^2 I_L(qr_<)K_L(qr_>)/\epsilon_0$ is the Coulomb interaction of two electrons on the ith and jth shells, with the radii r_i and r_j, respectively. $r_<(r_>)$ represents the smaller (larger) of r_i and r_j. $\chi_j v_j^{\mathrm{eff}}$ is recognized to be the induced charges on the jth shell. The external potential or the distribution of the probing electron would affect the effective potential and thus the intensity of the loss spectrum. However, the main characteristics of the low-frequency plasmon are hardly affected by it, e.g., the q-dependent plasmon frequency. The probing electron here is assumed to be located on the ith shell. The effective potential in Eq. (3) is obtained from the known external potential. According to the Fermi golden rule, the transition rate $P(q,L,w)$ that the probing electron transfers (q,L,w) to the nanotube system is given by

$$\begin{aligned} P(q,L,w)&=\sum_{j=1}^{N}-\mathrm{Im}[\chi_j(q,L,w)]|v_j^{\mathrm{eff}}(q,L,w)|^2\\ &\equiv v_i^{\mathrm{ex}}(q,L,w)\mathrm{Im}\left[\frac{-1}{\epsilon^{\mathrm{eff}}(q,L,w)}\right]. \end{aligned} \tag{4}$$

Equation (4) defines a dimensionless quantity $\mathrm{Im}[-q/\epsilon^{\mathrm{eff}}(q,L,w)]$, which could be interpreted as the EELS intensity of an N-shell nanotube. It is also noticed that the dielectric function of an N-shell nanotube is an $N\times N$ matrix, which satisfies $\Sigma_j\epsilon_{ij}v_j^{\mathrm{eff}}=v_i^{\mathrm{ex}}$. The plasmon frequency could also be determined from $\det(\epsilon_{ij})=0$. $\mathrm{Im}[-1/\epsilon^{\mathrm{eff}}(q,L,w)]$ in Eq. (4) is mainly used in the calculations. It is basically similar to the loss spectrum ($\mathrm{Im}[-1/\epsilon(q,L,w)]$) of a single-shell nanotube.

The identical single-shell nanotubes could further form a 2D lattice.[16] The dielectric response of a nanotube bundle is complicated [Eqs. (B3′) and (B4); Appendix B]. But when the transferred momentum ($\mathbf{q}_\perp$) perpendicular to the tubular axis vanishes, the dielectric function is relatively simple. By the detailed analysis, the dielectric function in the absence of $\mathbf{q}_\perp$ is expressed by

$$\epsilon(q,w)_{|\mathbf{q}_\perp=0}=\epsilon_0-2\pi N_a V(q;3\mathrm{D})\chi(q,L=0,w), \tag{5}$$

where $V(q;3\mathrm{D})=4\pi e^2/q^2$ is the Coulomb interaction of a 3D EGS, and N_a is the nanotube number per area. ϵ in Eq. (5) is only related to $\chi(q,L=0,w)$ of an isolated nanotube. This result clearly illustrates that the $L=0$ mode is the only excitation channel, when the external electric field is parallel to the nanotube axis. Since the low-frequency plasmon in a metallic nanotube only exists in the $L=0$ mode (Fig. 4), the above case $\mathbf{q}_\perp=0$ is suitable in understanding the effects due to the intertube interactions. The 3D Coulomb interaction in a nanotube bundle is very different from the 1D Coulomb interaction in a single-shell or multishell nanotube. The characteristics of the low-frequency plasmon are thus expected to be so.

III. THE LOW-FREQUENCY PLASMON

The dielectric function is further used to study the low-frequency excitation properties, e.g., the band-structure effect on the ϵ and q-dependent plasmon. The plasmon frequencies are evaluated for metallic single-shell and multishell nanotubes, and metallic nanotube bundles. They could be verified from the measurements of EELS.

A. A single-shell metallic nanotube

The metallic (21,0) nanotube is taken as a model system to see the low-frequency plasmon. The dielectric function of the $L=0$ excitations [Eq. (1)] is shown in Fig. 2(a) at $q=0.1$ Å^{-1} and $\Gamma=0$ eV. The real $[\epsilon_1(q,L,w)]$ and the imaginary $[\epsilon_2,(q,L,w)]$ parts of the dielectric function are, respectively, shown by the solid and dashed curves. ϵ_2 first exhibits a finite discontinuity (the first kind of singular structure) and then diverges in the form $1/\sqrt{w_0-w}$ (the second kind of singular structure). These structures basically reflect the features of the joint density of states [JDOS; $D(q,L,w)$], since $\epsilon_2(q,L,w)$ is proportional to it. JDOS is given by

$$D(q,L,w)=\left|\frac{\partial w_{vc}(J,k_y;q,L)}{\partial k_y}\right|^{-1}_{w_{vc}=w}. \tag{6}$$

JDOS is closely related to the energy dispersion relations, and so does ϵ_2. For a metallic nanotube, all subbands have parabolic profiles except the linear subbands (denoted by J_a's) intersecting at E_F. The linear J_a subband [Eq. (A4)] is well approximated by the relation

$$E^c(J_a,k_y)\approx\gamma_0\left\{\left|\frac{3bk_y}{2}\right|-\left|\frac{3bk_y}{2}\right|^3\Big/24\right\}. \tag{7}$$

The excitation energy, $w_{vc}(J_a,k_y;q,L=0)$, between the two linear subbands is a minimum for the $k_y=0$ state and a local maximum for the $k_y=-q/2$ state. These two critical points may be too close to distinguish each other at smaller q's, e.g., $q=0.01$ Å^{-1}. The k_y-dependent dispersion relation

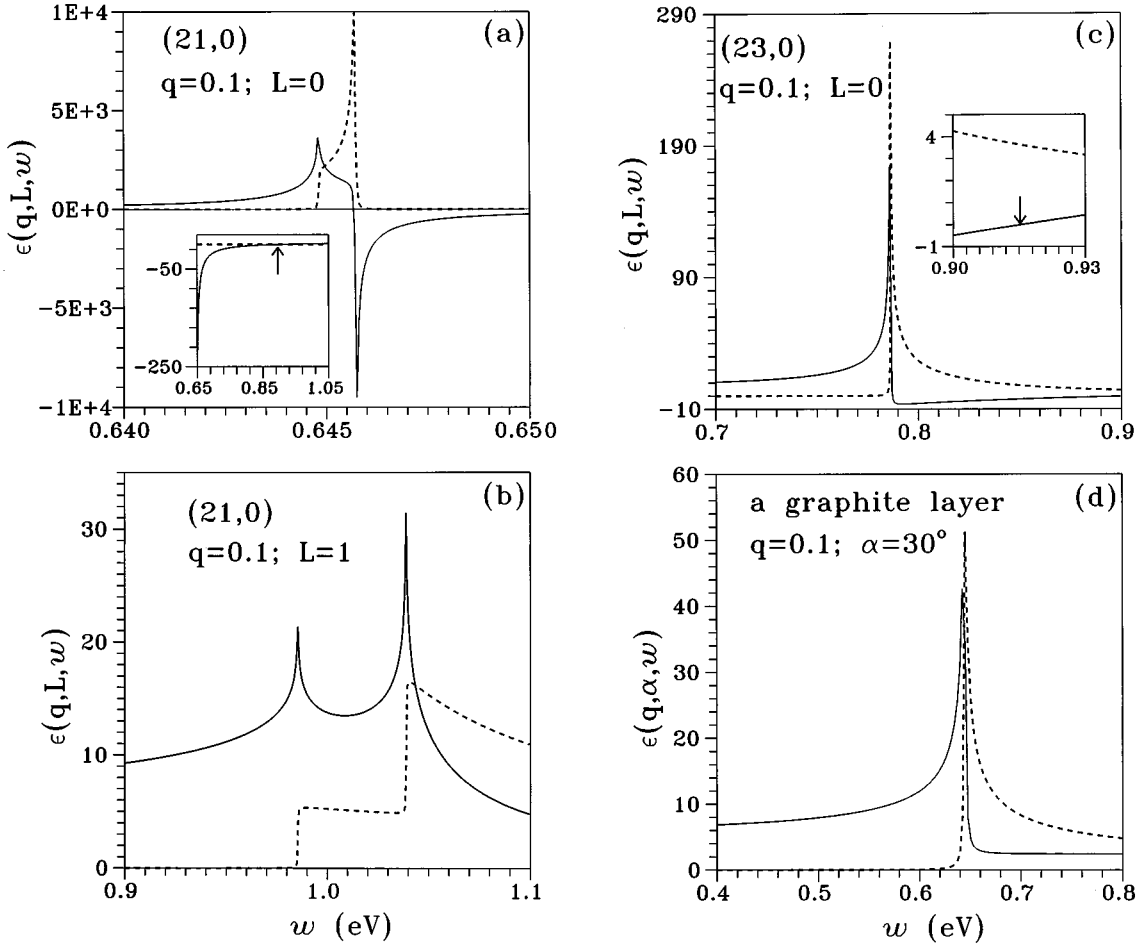

FIG. 2. The real (ϵ_1) and the imaginary (ϵ_2) parts of the dielectric function are, respectively, shown by the solid and the dashed curves. They are calculated at $\Gamma=0$ eV, $q=0.1$ Å^{-1}, and (a) $L=0$ for the (21,0) nanotube, (b) $L=0$ for the (21,0) nanotube, (c) $L=0$ for the (23,0) nanotube, and (d) $\alpha=30°$ for the graphite layer. The arrows point at the zeros of ϵ_1.

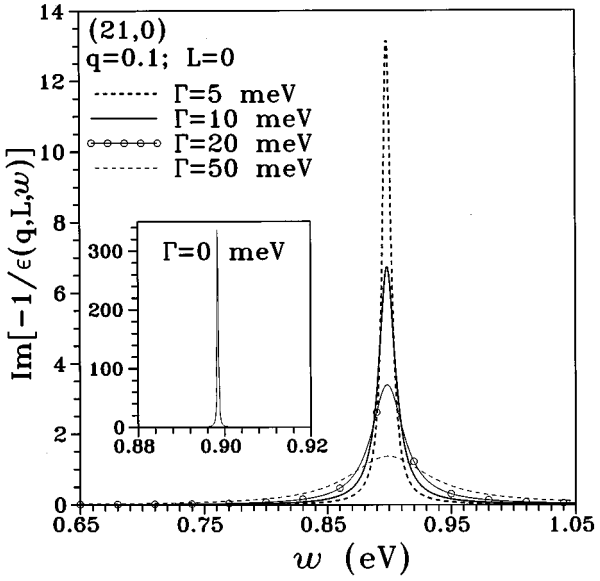

FIG. 3. The low-frequency EELS of the (21,0) nanotube. They are calculated at various Γ's. The inset shows the EELS at $\Gamma=0$ eV.

near the minimum is linear, but that near the local maximum is parabolic (the concave-downward form). These two kinds of dispersion relations, as calculated from Eq. (6), would induce the finite discontinuity and the square-root divergency $1/\sqrt{w_0-w}$, respectively. From the singular structures in ϵ_2, those in ϵ_1 could be obtained by using the Kramers-Kronig relations. ϵ_1, as shown in Fig. 2(a), exhibits the positive logarithmic divergency and then the negative square-root divergency $-1/\sqrt{w-w_0}$. Apparently, ϵ_1 must have zeros in the neighborhood of the negative square-root divergency. Zeros of ϵ_1, if they are at where $\epsilon_2\rightarrow 0$, are associated with plasmons. Here ϵ_1 could vanish at $\epsilon_2\rightarrow 0$ [inset in Fig. 2(a)], therefore, there is a sharp plasmon peak in EELS (inset in Fig. 3). In addition, the negative square-root divergency in ϵ_1 is similar to that causing the π plasmon.[15]

ϵ of the $L=1$ excitations is shown in Fig. 2(b) to see the L dependence. For the low-frequency inter-π-band excitations, electrons are excited from the linear to the parabolic subbands or vice versa. The excitation energies have a minimum and a local minimum in the energy-wave-vector space. Furthermore, the k_y-dependent dispersion relations near such critical points are linear. These linear dispersion relations, as stated above, could induce the first kind of singular structure in ϵ, the finite discontinuity in ϵ_2, and the positive logarith-

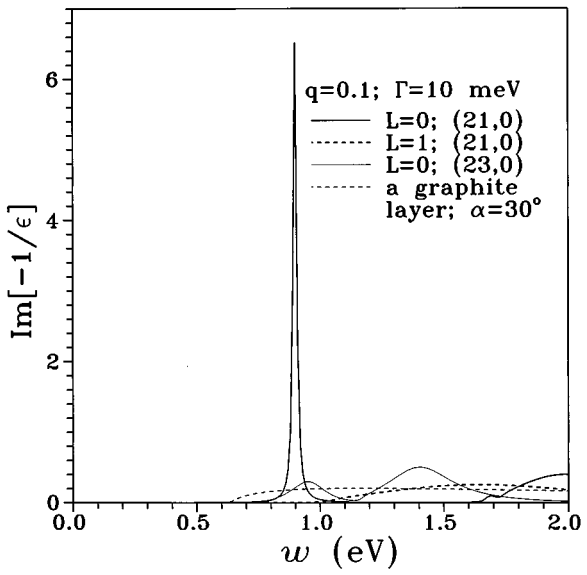

FIG. 4. The EELS corresponding to the dielectric functions shown in Fig. 2, but calculated at $\Gamma=10$ meV.

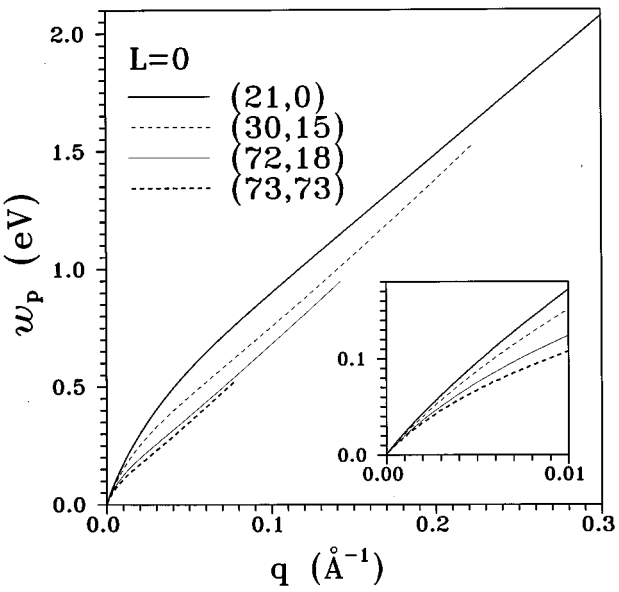

FIG. 5. The low-frequency plasmon of the $L=0$ mode. The q-dependent plasmon frequencies are shown for four metallic nanotubes: (21,0), (30,15), (72,18), and (73,73). The inset shows the details at small q's.

mic divergency in ϵ_1. ϵ_1 does not vanish at $\epsilon_2\rightarrow 0$, so that there is no plasmon peak in EELS (the heavy dashed curve in Fig. 4). Similar results are obtained for other $L\neq 0$ excitations. Hence the low-frequency plasmon does not have $L\neq 0$ modes.

We take the semiconducting (23,0) nanotube as a model system to see the dependence of the low-frequency plasmon on band structure. The parabolic bonding energy bands concave downwards at the band edge ($k_y=0$) for $E^v>-\gamma_0$, and vice versa [Fig. 1(b)]. The low-frequency excitations of $L=0$ come from the former, and the dispersion relation of w_{vc} with k_y is in the quadratic form $w_0+Ck_y^2$. Such kind of k_y dependence could cause the third kind of singular structure in ϵ [Fig. 2(c)], the square-root divergency $1/\sqrt{w-w_0}$ in ϵ_2, and $1/\sqrt{w_0-w}$ in ϵ_1. The singular structure in ϵ_1 might accompany the negative and the vanishing ϵ_1 at $w>w_0$ [inset in Fig. 2(c)]. It is also noticed that ϵ_1 is not vanishing at smaller q's, e.g., $q=0.01$ Å^{-1}. ϵ_1 possibly vanishes, but occurs at large ϵ_2. Therefore, a sharp plasmon peak does not appear in EELS (the light solid curve in Fig. 4). It means that a semiconducting nanotube could not exhibit the low-frequency plasmon.

$\epsilon(q,\alpha,w)$ of a graphite layer at $\alpha=30°$ is shown in Fig. 2(d) for comparison. The inter-π-band excitation from the K point [Fig. 1(c)] requires the minimum excitation energy, the threshold energy. The energy dispersion relation near the K point is linear and isotropic. By using these two characteristics, ϵ_2 and ϵ_1 are found to diverge in the forms $1/\sqrt{w-w_0}$ and $1/\sqrt{w_0-w}$ ($w_0=3\gamma_0 bq/2$), respectively.[22] ϵ exhibits the third kind of singular structure, as seen in a semiconducting nanotube [Fig. 2(c)]. $\epsilon_1\neq 0$ and ϵ_2 is large, which indicates that the low-frequency plasmon does not exist in a graphite layer (the light dashed curve in Fig. 4). The azimuthal angle α would affect ϵ, but the conclusion reached here remains the same. In short, there are three kinds of singular structures in ϵ, which basically reflect the π-band profiles near the Fermi level. Only the second kind of singular structure, the negative square-root divergency $-1/\sqrt{w-w_0}$ in ϵ_1 and the positive square-root divergency $1/\sqrt{w_0-w}$ in ϵ_2, could induce $\epsilon_1=0$ at $\epsilon_2\rightarrow 0$ and thus the low-frequency plasmon. It corresponds to the $L=0$ excitations in a metallic nanotube.

The EELS, defined as $\mathrm{Im}[-1/\epsilon]$, is further calculated for a closer study of the low-frequency plasmon. The $L=0$ excitations of a metallic nanotube would exhibit a very sharp plasmon peak, because ϵ_1 vanishes at $\epsilon_2\rightarrow 0$, e.g., EELS of the (21,0) nanotube (inset in Fig. 3). The sharp plasmon peak would be broadened by the energy width (Fig. 3). However, it remains pronounced even at large Γ's (e.g., $\Gamma=50$ meV), and the plasmon frequency is insensitive to Γ. The pronounced peak due to the low-frequency plasmon is expected to be observable from the measurements of REELS with high resolution ~ 10 meV.[10] Such a peak is shown to be absent in a semiconducting nanotube, a graphite layer, and even a metallic nanotube exhibiting the $L\neq 0$ excitations (Fig. 4), i.e., the low-frequency plasmon does not exist in them. The metallic and the semiconducting nanotubes have been predicted to exhibit the different magnetic,[5–7] transport,[8] and thermal[9] properties. Concerning the excitation properties studied here, the principal difference between them is the low-frequency plasmon. The measurements on the low-frequency plasmon would be very useful in distinguishing the electronic structure of a nanotube system.

The q-dependent behavior of the low-frequency plasmon is important in understanding its characteristics. The plasmon frequency $w_p(q,L=0)$ of the (21,0) nanotube is shown in Fig. 5 by the heavy solid curve. The low-frequency plasmon exhibits a strong dispersion relation with q, as seen in the π plasmon.[15] This result directly reflects the π-band characteristic, the strong wave-vector dependence. The strong q dependence means that the plasma oscillation along the tubular axis (the $L=0$ mode) behaves as a propagating wave, with a continuous wavelength $2\pi/q$. w_p increases

quickly at small q's as shown in the inset. From the linear energy band in Eq. (7), one can show that $w_p \propto q|\ln(qr)|^{1/2}$ at small q's. The low-frequency plasmon should belong to a 1D acoustic plasmon. Such q dependence is similar to that of a 1D EGS in QW's,[11] which implies that the free carriers in the linear subbands of a metallic nanotube resemble a 1D EGS. The similarity lies in the fact that the low-frequency excitation energy is essentially linear in q—whether the energy band has a linear or a quadratic dispersion relation.

In addition to the L dependence, whether a metallic nanotube exhibits an acoustic plasmon relies on q and r. The low-frequency plasmon could exist at $q \to 0$, but would disappear at large q's, e.g., $q_c \sim 0.3$ Å^{-1} for the (21,0) nanotube. When q is sufficiently large, the certain inter-π-band excitation except those from the linear subbands would make a large contribution to ϵ_2 (not shown) at $\epsilon_1 = 0$. The strong Landau damping thus results in the destruction of the low-frequency plasmon. The other metallic nanotubes exhibit the similar low-frequency plasmons. But for a larger nanotube (Fig. 5), the plasmon frequency is lower—mainly due to the weaker Coulomb interaction. Furthermore, it has more 1D subbands so that the low-frequency plasmon is relatively easily affected by the Landau damping, i.e., q_c is smaller for a larger nanotube. This result suggests that a smaller metallic nanotube is more suitable in verifying the low-frequency plasmon.

The low-frequency plasmon in a metallic nanotube is very different from the π plasmon in all carbon nanotubes.[15] There are certain important differences between them. First, the low-frequency plasmon is derived from the linear bands intersecting at E_F, but the π plasmon are concave-upward bonding energy below $-\gamma_0$. Consequently, the former depends on the π-band property near E_F, while the latter does not. They are, respectively, confined to the frequency range $w_p < 2$ eV and $w_p > 6$ eV. Second, the former only has the $L = 0$ mode, which is in great contrast to the latter with various L modes. Finally, the former belongs to an acoustic plasmon, which is similar to that of a 1D EGS. However, the latter is an optical plasmon, and it behaves as that of a 3D EGS.

The π-electronic excitations have been studied within the EGS model.[12–14,19] While the π electrons in the bonding energy bands[13,14,19] are modeled as an EGS, the π plasmon of $L = 0$ is predicted to belong to a 1D acoustic plasmon, i.e., w_p approaches zero at small q's. Such a result, understandably, only reflects the characteristics of a 1D EGS, but not those of a real π band. In fact, the $L = 0$ π plasmon has a finite frequency $w_p \sim 6$ eV at small q's.[15] Moreover, for the $L = 0$ mode, a metallic nanotube could exhibit the low-frequency plasmon as well as the π plasmon. The EGS model, which neglects the real band structure, might be inappropriate for the $L = 0$ excitations from the bonding energy bands. Metallic atoms could be further intercalated into carbon nanotubes,[23] so that there are additional electrons in the antibonding energy bands.[24] Within the EGS model,[12] such free carriers are predicted to be capable of exhibiting a 1D acoustic plasmon of $L = 0$, as seen in a metallic nanotube (without intercalation). A closer investigation including the real π band is needed. In short, the π-band structure plays an important role in the excitation properties of carbon nanotubes, which, thus, needs to be taken into consideration.

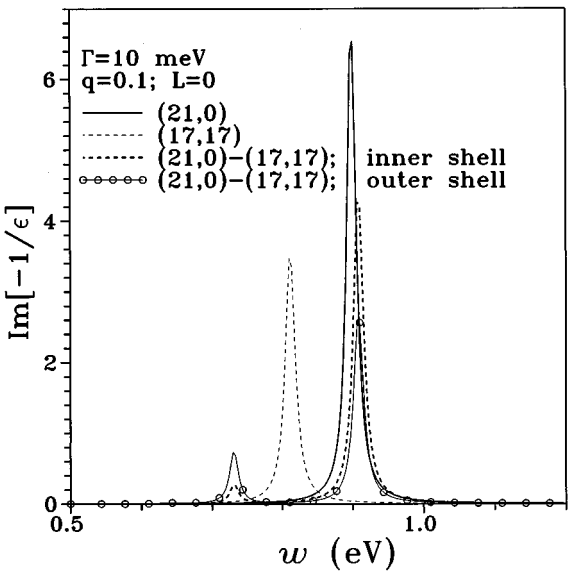

FIG. 6. The EELS of the nanotubes: (21,0), (17,17), and (21,0)-(17,17). They are calculated at $q = 0.1$ Å^{-1}, $L = 0$, and $\Gamma = 10$ meV. The heavy dashed and the solid-circled curves are the EELS, with the probing electron localized in the inner and outer nanotubes.

B. A metallic-metallic nanotube

The intertube coupling in a multishell system would make the low-frequency excitations more complicated, since charge fluctuations on one shell influence the charges on other shells. The metallic-metallic nanotube, (21,0)-(17,17), is taken as an example to see the coupling effect. EELS [Eq. (4)] is shown in Fig. 6 at $q = 0.1$ Å^{-1} and $L = 0$. The probing electron is supposed to be localized on the inner or the outer shell. There are two clear plasmon peaks in EELS. AP_1 denotes the acoustic plasmon with the higher frequency, and AP_2 that with the lower frequency. The different external potentials would affect the intensity of the EELS. However, they do not alter the main characteristics of the low-frequency plasmons. For example, the plasmon frequencies remain almost the same, and AP_1 exhibits the strongest spectrum at low-frequency range. The measured EELS is roughly estimated to be between these two kinds of spectra. The intensity of AP_1 is much stronger than that of AP_2. That AP_1 and AP_2, respectively, correspond to coherent and incoherent oscillations of free carriers on different shells could explain this result. As a result the low-frequency plasmon with the highest frequency is most easily observed in the EELS.

The low-frequency plasmons in the uncoupled (21,0) and (17,17) nanotubes, as seen in Fig. 6, are clearly affected by the intertube Coulomb interactions. At small q's, the coupling effect is appreciable, mainly due to the strong intertube interactions $[V(q,L;r_1,r_2)]$. They significantly modify the q-dependent plasmon frequencies as shown in Fig. 7. They might change the q dependence from $q|\ln(qr)|^{1/2}$ into q, e.g., AP_2 at small q's (inset in Fig. 7). But on the other hand, the intertube interactions are negligible at large q's. AP_1 would become the low-frequency plasmon of the inner nanotube,

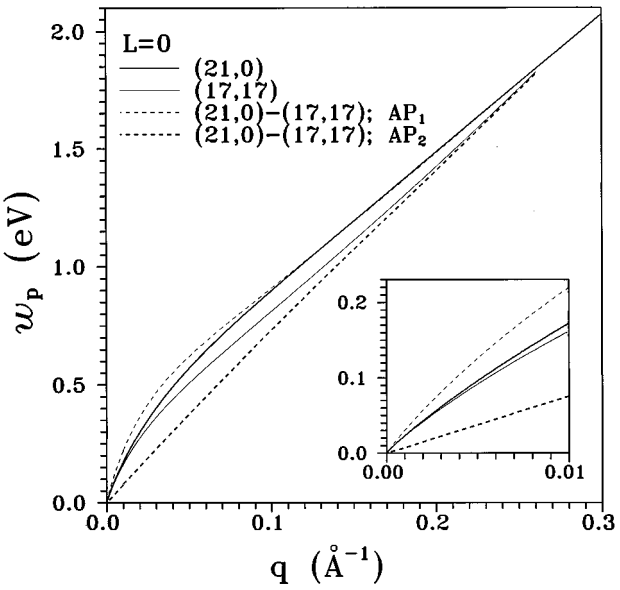

FIG. 7. Same plot as Fig. 5, but for the nanotubes: (21,0), (17,17), and (21,0)-(17,17). The light and the heavy dashed curves are the two acoustic plasmons of the (21,0)-(17,17) nanotube.

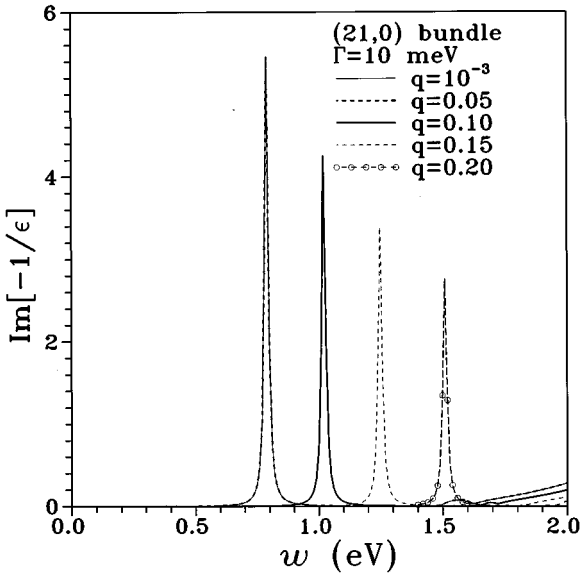

FIG. 8. The EELS of the (21,0) nanotube bundle is calculated at $\Gamma=10$ meV and different q's.

and AP_2 that of the outer nanotube. That is to say, each metallic nanotube exhibits the separate plasmon.

There are more plasmon modes as the shell number of metallic nanotubes increases. The plasmon with the highest frequency, as stated above, exhibits the strongest spectrum. And then, the plasmon peaks quickly decline in the decreasing of plasmon frequency. For example, the third acoustic plasmon in the (21,0)-(17,17)-(22,22) nanotube, as compared with AP_1 and AP_2, might be too weak to be observed in the EELS. AP_1 and AP_2 are thus expected to cause the main peak structures in the loss spectrum of a metallic multishell nanotube. In short, the intertube coupling would markedly modify the acoustic plasmons in separate metallic nanotubes. This feature is absent in semiconductor QW's.[11]

C. A metallic nanotube bundle

The Coulomb interaction changes from the 1D into the 3D form, when the same single-shell nanotubes are packed in the lattice structure. Hence the characteristics of the low-frequency plasmon would change thoroughly. The dielectric function in Eq. (5) is used to study the effects of the intertube interactions on the low-frequency plasmon. We mainly focus on the case $\mathbf{q}_\perp=0$.

The metallic nanotubes are assumed to be located in accord with a triangular lattice with the lattice constant d (=3.15 Å).[16] The bundle thus has one nanotube per $2/\sqrt{3}(2r+d)^2$. EELS of the (21,0) nanotube bundle is shown in Fig. 8 at various q's and $\Gamma=10$ meV. The sharp peaks, as seen in an isolated nanotube (Fig. 4), are due to the collective excitations of the free carriers. The plasmon frequency clearly increases with q. When q vanishes, EELS exhibits a prominent plasmon peak at a finite frequency (the light solid curve). The low-frequency plasmon in a nanotube bundle is indicated to be an optical plasmon. It differs greatly from the acoustic plasmon in a metallic single-shell or multishell nanotube. This feature is associated with the very strong intertube interaction at small q's.

The plasmon in a nanotube bundle is derived from the coherent plasma oscillations of all metallic nanotubes. Therefore, it is similar to the optical plasmon in a 3D EGS, but not the acoustic plasmon in a 1D EGS.[11] For example, the q-dependent plasmon frequency, as shown in Fig. 9, has the parabolic form w_0+Aq^2 at small q's. Moreover, the plasmon frequency at $q\rightarrow 0$ is approximately antiproportional to the nanotube radius, since the total free-carrier density is proportional to the nanotube density. This optical plasmon, as compared with the acoustic plasmon in an isolated nanotube (Fig. 5), has the higher frequency owing to the stronger Coulomb interaction. The intertube interaction is

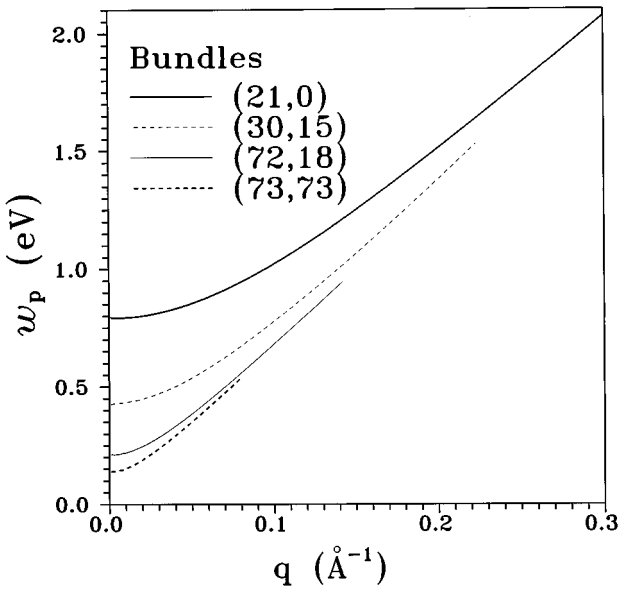

FIG. 9. The q-dependent plasmon frequencies of the metallic nanotube bundles: (21,0), (30,15), (72,18), and (73,73).

getting weak in the increasing of q's. Consequently the former would degenerate into the latter at large q's.

How the metallic nanotubes are arranged do not alter the main features of the low-frequency plasmon. The relevant nanotube density only affects the plasmon frequency. The closest packing form, the triangular lattice studied here, has the highest plasmon frequency. Other lattices, e.g., the tetragonal lattice, have the lower plasmon frequencies. The direction of the transferred momentum $(q,\mathbf{q}_\perp)$ also has an effect on the plasmon frequency. It even leads to significant changes in the primary features when $\mathbf{q}_\perp \gg q$. For example, the low-frequency plasmon would disappear at $q=0$ (Appendix B.) Hence, the optical plasmon in a metallic nanotube bundle exhibits the most obvious loss spectrum in the absence of $\mathbf{q}_\perp$.

The above-mentioned optical plasmon could be verified by the REELS or the optical spectrum. It is expected to exhibit a sharp peak in EELS and a Drudelike edge in reflectance spectrum. The measurements of the q-dependent EELS are more useful in understanding the main features. The bundle made up of the metallic nanotubes, as indicated from the measured resistivity,[16] exhibits the metallic behavior. The measurements on the optical plasmon could provide another kind of verification.

IV. CONCLUDING REMARKS

In this work, the low-frequency excitations in a single-shell and multishell carbon nanotube, a nanotube bundle, and a graphite sheet, are studied within the SCE approach. Whether the low-frequency plasmon exists depends on the band structure. The measurements on the excitation properties, together with the magnetic,[5–7] transport,[8] and thermal properties,[9] are useful in distinguishing the electronic structure of a nanotube system. A similar study could be further extended to the intercalated carbon nanotubes.[23,24]

A low-frequency plasmon is found to exist in a metallic nanotube, but not a semiconducting nanotube or a graphite layer. That a metallic nanotube owns free carriers in the linear subbands is the main reason. Such a plasmon, which corresponds to the $L=0$ excitations, is a 1D acoustic plasmon. It behaves as that of a 1D EGS. However, it is quite different from the π plasmons in all carbon nanotubes,[15] e.g., the cause of plasmon and the q-dependent behavior. The low-frequency plasmon induces a very pronounced peak in EELS, which is expected to be observable from the measurements of the high-resolution REELS.[10] For a smaller metallic nanotube, it could exist at larger q's, and its frequency is higher. Hence, the smaller carbon nanotubes are more suitable in the experimental verifications.

Intertube Coulomb interactions are very important for a metallic multishell nanotube and a metallic nanotube bundle. They strongly affect the low-frequency plasmon. The intertube coupling among coaxial nanotubes significantly modifies the acoustic plasmons in separate metallic nanotubes. There are more acoustic plasmons as the shell number of metallic nanotubes grows. The acoustic plasmons with the higher frequencies are expected to display the primary peak structures in the loss spectrum. When the identical metallic nanotubes form a lattice, the low-frequency plasmon would change into an optical plasmon, and behave like that in a 3D EGS. The reflection EELS and the optical spectrum could be used to verify such kind of plasmon.

It should be noticed that metallic nanotubes could exhibit the metallic behavior even in the absence of intercalation or doping,[2–4] e.g., the low-frequency plasmon. On the other hand, metallic atoms, e.g., K and Rb, have been successfully intercalated into carbon nanotubes.[23] Many free carriers, which occupy the antibonding energy bands, are predicted to exist in various carbon nanotubes.[24] Such electrons due to intercalation might exhibit the richer excitation spectra. For example, they are expected to exhibit the acoustic plasmon of $L=0$ and the optical plasmons of $L\neq 0$.[12] These plasmons will be investigated in a further study.

ACKNOWLEDGMENTS

This work was supported in part by the National Science Council of Taiwan, Republic of China under Grants Nos. NSC 86-2112-M-009-006 and NSC 86-2112-M-007-003.

APPENDIX A

The π-band structure is simply reviewed. The π band of a graphite layer is calculated from the tight-binding model.[18] The Bloch states are described by the two tight-binding functions built from the $2p_z$ orbitals, $\phi_z(\mathbf{r}')$:

$$U_{i\mathbf{k}'}(\mathbf{r}')=C\sum_{\mathbf{R}_n} e^{i\mathbf{k}'\cdot(\mathbf{R}_n+\tau i)}\phi_z(\mathbf{r}'-\mathbf{R}_n-\tau_i), \quad i=1,2. \tag{A1}$$

$\mathbf{k}'$ is the 2D wave vector, C is the normalization factor, and $\mathbf{R}_n$ is the lattice vector. τ_1 and τ_2 define the positions of carbon atoms in a unit cell. Diagonalizing the Hamiltonian with only the nearest-neighbor interactions taken into consideration, the energy dispersions of a graphite layer are

$$E^{c,v}\left(k_{x'},k_{y'}\right)=\pm\gamma_0\left\{1+4\cos\left(\frac{3bk_{y'}}{2}\right)\cos\left(\frac{\sqrt{3}bk_{x'}}{2}\right)+4\cos^2\left(\frac{\sqrt{3}bk_{x'}}{2}\right)\right\}^{1/2}, \tag{A2}$$

and the corresponding wave functions are

$$\Psi^{c,v}_{\mathbf{k}'}(\mathbf{r}')=\frac{1}{\sqrt{2}}\left\{U_{1\mathbf{k}'}(\mathbf{r}')\mp\frac{H^*_{12}(k_{x'},k_{x'})}{|H_{12}(k_{x'}k_{y'})|}U_{2\mathbf{k}'}(\mathbf{r}')\right\}. \tag{A2$'$}$$

The superscript c (v) represents the antibonding (bonding) band which is located above (below) the Fermi level $E_F=0$. $\gamma_0=3.033$ eV is the resonance integral.[4] $H_{12}=-\gamma_0\Sigma_{i=1}^{3}e^{-i\mathbf{k}'\cdot\mathbf{r}_i}$ is the nearest-neighbor Hamiltonian matrix element.

A similar calculation is applied to a cylindrical carbon nanotube, but with the periodical boundary condition along the rolled direction. The angle between the rolled direction (x axis) and the x' axis is the chiral angle θ. The relationship between wave vectors (k_x,k_y) of a carbon nanotube and those $(k_{x'},k_{y'})$ of a graphite layer is described by[7]

$$k_{x'}=k_x\cos\theta-k_y\sin\theta \tag{A3}$$

and

$$k_{y'} = k_x \sin\theta + k_y \cos\theta. \tag{A3'}$$

Equations (A2) and (A2′), together with the above transformation, describe the π band of a carbon nanotube. The axial wave vector k_y is confined within the first BZ. The transverse wave vector satisfying the periodic boundary condition is $k_x = J/r$, where $J = 1,2,\ldots,N_u/2$; N_u is the atom number in a primitive unit cell. J serves as the subband index, which is the angular momentum of electrons circulating a nanotube. The energy dispersions and the Bloch functions are used in the calculations of the dielectric function (Sec. II). For a zigzag $(m,0)$ nanotube, the energy dispersions are expressed by

$$E^{c,v}(J,k_y) = \pm\gamma_0 \left\{ 1 + 4\cos\left(\frac{3bk_y}{2}\right)\cos\left(\frac{J\pi}{m}\right) + 4\cos^2\left(\frac{J\pi}{m}\right)\right\}^{1/2}. \tag{A4}$$

$J_a = 2m/3$ and $4m/3$ are the linear subbands intersecting at $E_F = 0$.

APPENDIX B

The dielectric function of a nanotube bundle is evaluated in this appendix. The bundle made up of the identical single-shell nanotubes is packed in a periodical 2D structure. Bloch functions have the periodicity $\mathbf{R}_{\perp,m}$ of the 2D lattice and are expressed by

$$|\alpha\rangle = |\mathbf{k}_\perp; J, k_y, h\rangle = C' \sum_{\mathbf{R}_{\perp,m}} \exp(i\mathbf{k}_\perp \cdot \mathbf{R}_{\perp,m}) \Psi^h_{J,k_y}(\mathbf{r}_\perp - \mathbf{R}_{\perp,m}), \tag{B1}$$

where Ψ^h_{J,k_y} $(h = c,v)$ is the Bloch function of an isolated nanotube. $\perp$ denotes the vector perpendicular to the tubular axis. For example, $\mathbf{k}_\perp$ is perpendicular to k_y. When an external potential $V^{\rm ex}(q,\mathbf{q}_\perp,w)$ is applied, it would induce charge fluctuations on all nanotubes. The induced potential due to the screening charges is obtained from Poisson's equation:

$$V^{\rm in}(q,\mathbf{q}_\perp,w) = V(q,\mathbf{q}_\perp) n^{\rm in}(q,\mathbf{q}_\perp,w). \tag{B2}$$

$V(q,\mathbf{q}_\perp) = 4\pi e^2/(q^2 + \mathbf{q}_\perp^2)$ is the Coulomb interaction of a 3D EGS. The induced charge density within the linear response[17] is

$$n^{\rm in}(q,\mathbf{q}_\perp,w) = \chi(q,\mathbf{q}_\perp,w) V^{\rm eff}(q,\mathbf{q}_\perp,w), \tag{B3}$$

and

$$\chi(q,\mathbf{q}_\perp,w) = 2\sum_{\alpha,\alpha'} |\langle\alpha'|e^{iqx} e^{i\mathbf{q}_\perp\cdot\mathbf{r}_\perp}|\alpha\rangle|^2 \times \frac{f^0(E_\alpha) - f^0(E_{\alpha'})}{E_\alpha - E_{\alpha'} - (w + i\Gamma)}. \tag{B3'}$$

f^0 is the Fermi-Dirac function. E_α is the energy dispersion of each nanotube, which depends on (J,k_y,h). The induced charge density is proportional to the effective potential, and the coefficient is the response function $\chi(q,\mathbf{q}_\perp,w)$ [Eq. (B3′)].

The effective potential is the sum of the external potential and the induced potential. The dielectric function is given by

$$\epsilon(q,\mathbf{q}_\perp,w) = \frac{V^{\rm ex}(q,\mathbf{q}_\perp,w)}{V^{\rm eff}(q,\mathbf{q}_\perp,w)} = \epsilon_0 - V(q,\mathbf{q}_\perp)\chi(q,\mathbf{q}_\perp,w). \tag{B4}$$

The square of the matrix element in the response function [Eq. (B3′)] is complex, and so is the dielectric response. However, the response function in the absence of $\mathbf{q}_\perp$ could be further reduced to

$$\chi(q,\mathbf{q}_\perp = 0,w) = 2\pi N_a \chi(q,L=0,w), \tag{B5}$$

where $\chi(q,L=0,w)$ is the response function of an isolated nanotube. When the external electric field is parallel to the tubular axis, the response function of a nanotube bundle is the superposition of the $L=0$ excitations of all nanotubes. This case is very suitable in understanding the effects of the intertube interactions on the $L=0$ low-frequency plasmon. On the other hand, the $L=1$ excitations from all nanotubes are the principal response of a nanotube bundle as q vanishes. This result could be obtained from the small-$\mathbf{q}_\perp$ expansion in Eq. (B3′) and $\chi(q,L=0,w) \propto q^2$ at small q's. Apparently, the low-frequency plasmon does not exist under such a case. For any q and $\mathbf{q}_\perp$, the electronic excitations in a nanotube bundle are mainly related to the $L=0$ and 1 modes. $\mathbf{q}_\perp = 0$ should be the case, which the effects of the intertube interactions on the $L=0$ excitations are most obvious. That is to say, the $L=0$ excitations of an isolated nanotube are most strongly modified by the intertube interactions. The study is focused on the case $\mathbf{q}_\perp = 0$.

[1] S. Iijima, Nature (London) **354**, 56 (1991).
[2] J. W. Mintwire *et al.*, Phys. Rev. Lett. **68**, 63 (1992); C. T. White *et al.*, Phys. Rev. B **47**, 5485 (1993).
[3] N. Hamada, S. I. Sawada, and A. Oshiyama, Phys. Rev. Lett. **68**, 1579 (1992).
[4] R. Saito *et al.*, Appl. Phys. Lett. **60**, 2204 (1992); Phys. Rev. B **46**, 1804 (1992).
[5] H. Ajiki and T. Ando, J. Phys. Soc. Jpn. **62**, 1255 (1993); **62**, 2470 (1993).
[6] J. P. Lu, Phys. Rev. Lett. **74**, 1123 (1995).
[7] M. F. Lin and K. W.-K. Shung, Phys. Rev. B **52**, 8423 (1995).
[8] R. A. Jishi, M. S. Dresselhaus, and G. Dresselhaus, Phys. Rev. B **48**, 11 385 (1993).
[9] M. F. Lin and K. W.-K. Shung, Phys. Rev. B **54**, 2896 (1996).
[10] A. A. Lucas, J. Phys. Chem. Solids **53**, 1415 (1992).
[11] S. D. Sarma and Wu-Yan Lai, Phys. Rev. B **32**, 1401 (1985); Q. Li and S. D. Sarma, *ibid.* **40**, 5860 (1989).
[12] M. F. Lin and K. W.-K. Shung, Phys. Rev. B **47**, 6617 (1993).

[13] P. Longe and S. M. Bose, Phys. Rev. B **48**, 18 239 (1993).
[14] C. Yannouleas *et al.*, Phys. Rev. B **53**, 10 225 (1996); **50**, 7977 (1994).
[15] M. F. Lin *et al.*, Phys. Rev. B **53**, 15 493 (1996); J. Phys. Soc. Jpn. **66**, 757 (1997).
[16] A. Thess *et al.*, Science **273**, 483 (1996).
[17] H. Ehrenreich and M. H. Cohen, Phys. Rev. **115**, 786 (1959).
[18] P. R. Wallace, Phys. Rev. **71**, 622 (1947).
[19] P. S. Davids *et al.*, Phys. Rev. B **49**, 5682 (1994); **51**, 4557 (1995).
[20] E. A. Taft and H. R. Philipp, Phys. Rev. **138**, A197 (1965).
[21] N. D. Mermin, Phys. Rev. B **1**, 2362 (1970).
[22] K. W.-K. Shung, Phys. Rev. B **34**, 979 (1986).
[23] O. Zhou *et al.*, Science **263**, 1744 (1994).
[24] Y. Miyamoto *et al.*, Phys. Rev. Lett. **74**, 2993 (1995); A. Rubio *et al.*, Phys. Rev. B **53**, 4023 (1996).